24th INTERNATIONAL CONGRESS ON SOUND AND VIBRATION
23–27 July 2017, London

ICSV24
23-27JULY 2017
LONDON CALLING

PARAMETRIC SENSITIVITY ANALYSIS FOR PREMIXED SWIRLING M-FLAMES

Calum S. Skene and Peter J. Schmid
Imperial College London, Department of Mathematics, South Kensington, London, UK
email: calum.skene11@imperial.ac.uk

A numerical study is carried out to determine the linear optimal response of an axisymmetric premixed M-flame to periodic forcing. Direct numerical simulations are undertaken on the reactive Navier-Stokes equations. By solving these equations with selective frequency damping, we can obtain steady M-flame base flows about which our linear analysis is performed. The linear and adjoint operators are obtained by modular automatic differentiation of the full non-linear code. These operators enable us to find the optimal harmonic forcing and its corresponding output by performing a singular value decomposition on the resolvent.

As each singular value decomposition is computationally expensive, we seek to extract a maximum amount of information from a single decomposition. Using a first-order accurate relation between the change in a singular value and a parametric change in the resolvent matrix, we easily and efficiently obtain sensitivities of the singular values with respect to forcing frequency and Reynolds numbers while avoiding additional singular value calculations.

Using these tools, we carry out an input-output analysis for the response of an M-flame to harmonic forcing. Parametric sensitivities for the optimal gains are also determined for variations in the mean flow swirl, with special emphasis on frequency shifts for the optimal amplification rates.

Keywords: premixed flames, thermoacoustic instabilities, adjoints, frequency response

1. Introduction

Combustion instabilities are a large problem in industry today, affecting gas turbines[1], propulsion systems[2] and many other applications. Often the type of combustion that would provide reasonable stability such as diffusion-flame combustors produce unacceptable levels of NOx leading to the development of other techniques such as lean premixed combustors (LPCs) which significantly reduce NOx levels. Unfortunately LPCs are particularly susceptible to thermo-acoustic instabilities meaning that these combustors must be operated below their true operational efficiency or be at risk of failure.

Even though combustion instabilities can be explained simply as the resonance between unsteady heat release and pressure perturbations via the Rayleigh criterion [3], the mechanisms leading to this resonance are often unclear. A lack of understanding of these mechanisms can lead to devices being designed and built susceptible to instability, which must be managed using control techniques. In both cases, the design or control of a combustion system needs a detailed understanding of the governing instabilities.

Swirl injectors are common in combustion, hence much research has been undertaken in understanding the effect of swirl, some of which has been collected into a review article by Huang and Yang[4]. In particular a numerical study using LES techniques has been used to study the effect of swirl on combustion dynamics [5]. It was found that increasing the inlet swirl creates a vortex-breakdown-induced central toroidal recirculation zone (CTRZ) providing a flame stabilisation mechanism. This stabilisation phenomenon explains why most LPC turbines utilise swirl injectors.

We intend to carry out a study of the linear response of a flame to harmonic forcing. This may seem reminiscent of a transfer function analysis, however we do not restrict ourselves to a point-wise forcing or response. Instead we look at how the resolvent operator maps global structures to global structures. Moreover, we do not specify the structure for the forcing or the output (except by a windowing in space) but allow the dynamics to choose the forcing that produces the maximum response possible. This allows us to carry out an input-output analysis to identify the responsive parts of the equations that lead to amplification and to see what flow dynamics are efficiently magnified. In particular, the effect of mean flow swirl will be studied, allowing us to quantify how increasing the mean flow swirl changes the dynamics, leading to stabilisation.

Our proposed study uses a reactive DNS solver [6] that is efficiently and accurately linearised [7] to provide the linear operator together with its adjoint. Using the linearised equations, we can probe directly into the linear response of our stabilised base-flow which is an M-flame at a given swirl number. The optimal forcing that provides the largest growth in the forced response is found for a variety of forcing frequencies allowing us to see which frequencies the flame is susceptible to. In addition, sensitivity of the growth rates can be evaluated with respect to flow parameters, providing insight into how the parameters affect instabilities. Similar studies have been conducted to evaluate the noise generated by an aerofoil [8] and to provide insight into pressure generation from a non-swirled premixed conical flame [9].

2. Governing Equations

The reactive Navier-Stokes equations [10] are given in terms of the non-dimensional Reynolds (Re), Prandtl (Pr), Lewis (Le) and Mach (Ma) numbers as

$$\begin{aligned}
\frac{\partial \rho}{\partial t} &= -\nabla \cdot (\rho \mathbf{u}) && (1)\\
\frac{D\rho\mathbf{u}}{Dt} &= -\nabla P + \frac{1}{\mathrm{Re}}\nabla \cdot \boldsymbol{\tau}, && (2)\\
\rho\frac{DE}{Dt} &= \frac{-1}{(\gamma-1)\mathrm{PrReMa}^2}\nabla^2 T - \nabla \cdot (P\mathbf{u}) + \frac{1}{\mathrm{Re}}\nabla \cdot (\boldsymbol{\tau}\cdot\mathbf{u}) + \mathcal{Q}'\dot{\omega}_f, && (3)\\
\frac{\partial \rho Y}{\partial t} &= -\nabla \cdot (\rho \mathbf{u} Y) - \dot{\omega}_f + \frac{1}{\mathrm{LePrRe}}\nabla \cdot (\rho \nabla Y), && (4)
\end{aligned}$$

where γ is the specific heat ratio. Equations (1), (2) and (3) are the common compressible Navier-Stokes equations for the density ρ, pressure P, temperature T, energy E and velocity $\mathbf{u}$ with the stress tensor denoted as τ. The energy equation (3) has an added term $\mathcal{Q}'\dot{\omega}_F$ to account for energy released during chemical reactions with $\mathcal{Q}'$ being the heat release per unit mass of fuel. Equation (4) is the species equation for the fuel mass fraction Y.

The non-dimensionalisation used is

$$\begin{aligned}
\mathbf{x} &= \frac{\hat{\mathbf{x}}}{L}, \quad \rho = \frac{\hat{\rho}}{\rho_0}, \quad T = \frac{\hat{T}}{T_0}, \quad E = \frac{\hat{E}}{U^2},\\
\mathbf{u} &= \frac{\hat{\mathbf{u}}}{U}, \quad P = \frac{\hat{P}}{\rho_0 U^2}, \quad Y = \frac{\hat{Y}}{Y_0} \quad t = \frac{\hat{t}}{L/U},
\end{aligned}$$

where hats denote the corresponding dimensional variables. The reference scales used correspond to the values for the fresh gas in the inlet tube, with the length scale L being the inlet tube radius r_1 shown in figure (1) and the reference velocity U being the injection velocity of the fresh gas at $r = -10$. Y_0 represents the fuel mass fraction in the fresh gases which ensures the range of the variable Y from 1 in the fresh gases to 0 in the burnt gases. The values for the reference density, dynamic viscosity and specific heat capacity are taken to correspond to the values that air attains at our reference temperature of $T_0 = 300K$.

A simplified one-step, irreversible chemical model [11] between two species (fuel and air) is used. By considering a very lean configuration (i.e. the equivalence ratio $\phi \ll 1$) we only need the fuel mass fraction to calculate the reaction rate $\dot{\omega}_f$ in the species and energy equations. This rate is given by an Arrhenius law

$$\dot{\omega}_f = A\rho Y_0 Y \exp(-T_a/T), \tag{5}$$

where A is a constant and T_a is the activation temperature. We consider the total non-chemical energy which can be broken down into the sum of the kinetic and sensible energies

$$E = \frac{1}{2}\mathbf{u}\cdot\mathbf{u} + \frac{P}{\rho(\gamma-1)}. \tag{6}$$

In order to write the energy in the form given by (6) we assumed equal and constant heat capacities for all species and made use of the non-dimensionalised state equation for a perfect gas

$$P = \frac{\rho T}{\gamma \mathrm{Ma}^2}. \tag{7}$$

A further assumption is that the diffusion coefficients of both species are equal which allows us to use Fick's law to simply the species equation to (4).

For this study we will be using $\mathrm{Re} = 1461$ (based on L and U), $\mathrm{Pr} = 0.72$, $\mathrm{Le} = 1$, $\gamma = 1.4$ and $\mathrm{Ma} = 0.1$. These parameters were chosen to be as realistic as possible whilst keeping in mind that an increased Reynolds number or decreased Mach number will cause a DNS approach to be too computationally expensive. The biggest trade off is that our parameters make the velocity scale U large at $35\mathrm{ms}^{-1}$ and the length scale L small at 0.64mm. In order to accurately represent the flame under these conditions we set the Arrhenius pre-factor to 60368.2, the heat release Q' to 54664.9, the initial fuel mass fraction Y_0 to 0.025 and the non-dimensional activation temperature to 40. This gives a flame speed of $2.9\mathrm{ms}^{-1}$ and a flame width of 0.007mm ($\approx 1\%$ of the injection tube radius).

3. Numerical Code

The numerical code is a reactive axisymmetric DNS solver called CNS2D (**C**ombustion **N**avier-**S**tokes **2D**) that has been used in previous studies [6]. External libraries PETSc [12] and SLEPc [13] are used extensively for parallelisation.

An annular inlet tube provides fresh gases to a central cylindrical burning area that is open at its numerical boundary. Throughout this paper we are taking the radius of the central rod $r_2 = 3/11$ and the radius of the inlet tube $r_1 = 1$. The rod protrudes into region 1 by an amount of $x_1 = 2/11$. Characteristic (LODI) boundary conditions are used both at the inlet in region 0 and at the outlet in region 1[14]. The inflow boundary conditions are used to specify the inlet mass fraction, temperature

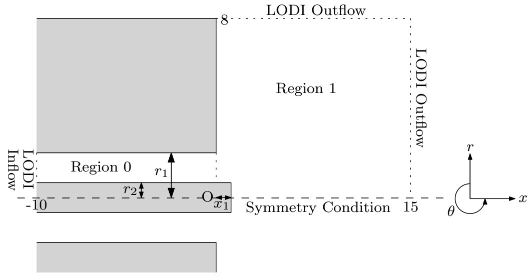

Figure 1: Numerical Domain

and velocity profile, whereas the outflow conditions are used to make sure we have no artificial wave reflection ensuring an open boundary configuration.

As we are interested in investigating mechanisms leading to acoustics and their production, it is of paramount importance that we treat waves carefully. To this end derivatives are taken using high order, low dissipative and low dispersive schemes [15]. In addition to the outflow conditions we further ensure that outgoing waves are not reflected by coarsening the grid far from the flame region where chemical reactions are taking place and a fine mesh is needed for proper treatment.

Due to the nature of our geometry, cylindrical polar coordinates (x, r, θ) are used with the velocity defined as $\mathbf{u} = u\mathbf{e}_x + v\mathbf{e}_r + w\mathbf{e}_\theta$. In this coordinate system the Navier-Stokes equations are solved in their conservative form

$$\frac{\partial \mathbf{q}}{\partial t} = \boldsymbol{\mathcal{N}}(\mathbf{q}), \tag{8}$$

where $\boldsymbol{\mathcal{N}}$ is the non-linear Navier-Stokes operator and the state $\mathbf{q} = (\rho, \rho u, \rho v, \rho w, \rho E, \rho Y)$.

The non-linear solver solves the axisymmetric equation (8) i.e. $\partial_\theta \equiv 0$. Using this non-linear solver we are able to find axisymmetric base-flows $\mathbf{q}_0$ where $\boldsymbol{\mathcal{N}}(\mathbf{q}_0) = 0$, using selective frequency damping [16] to force the state to a steady solution despite the flow being convectively unstable. Once a base-flow is found we can investigate the linear dynamics by linearising $\boldsymbol{\mathcal{N}}(\mathbf{q})$ about the base-flow to find the linear operator. We can write the linear equations of motion as

$$\frac{\partial \mathbf{q}'}{\partial t} = \underbrace{\left.\frac{\partial \boldsymbol{\mathcal{N}}(\mathbf{q})}{\partial \mathbf{q}}\right|_{\mathbf{q}_0}}_{\mathbf{A}} \mathbf{q}', \tag{9}$$

The linear operator $\mathbf{A}$ and its adjoint $\mathbf{A}^H$ are both found through automatic differentiation of the non-linear routines which are written in a modular way [7].

4. Optimal forcing-output

Consider the linearised equations subjected to a force $\mathbf{f}$ at frequency ω,

$$\frac{\partial \mathbf{q}}{\partial t} = \mathbf{A}\mathbf{q} + \mathbf{f}e^{i\omega t}. \tag{10}$$

As $\mathbf{A}$ is found to be stable, $\mathbf{q}$ will eventually respond at the forcing frequency, therefore we can write $\mathbf{q} = \hat{\mathbf{q}}(t, x, r, \theta)e^{i\omega t}$. After factoring out the $e^{i\omega t}$ term we can rewrite equation (10) as

$$\frac{\partial \hat{\mathbf{q}}}{\partial t} = (\mathbf{A} - i\omega\mathbf{I})\hat{\mathbf{q}} + \mathbf{f} \tag{11}$$

From equation (11) it is easily seen that the steady solution $\hat{\mathbf{q}}_{\text{out}}$ satisfies the relation,

$$\hat{\mathbf{q}}_{\text{out}} = \mathbf{R}\mathbf{f}, \tag{12}$$

where $\mathbf{R} = (i\omega\mathbf{I} - \mathbf{A})^{-1}$ is the resolvent matrix.

We want to optimise the output $\hat{\mathbf{q}}_{\text{out}}$ for a unit-norm forcing $\mathbf{f}$ at frequency ω i.e., we seek the force

$$\mathbf{f}^{\omega}_{\text{opt}} = \text{arg}\max_{\mathbf{f}} \frac{||\mathbf{R}\mathbf{f}||}{||\mathbf{f}||}, \tag{13}$$

and its corresponding output $\hat{\mathbf{q}}^{\omega}_{\text{opt}} = \mathbf{R}\mathbf{f}^{\omega}_{\text{opt}}$. We will allow the forcing and output to consist of all flow variables but shall confine the forcing to region 0 with $-2.5 < x < -0.5$ by using the windowing matrix $\mathbf{L}_{\text{in}}$. Similarly the output will be confined to region 1 with $x > 0$ with the matrix $\mathbf{L}_{\text{out}}$. The output will be measured by the Chu norm [17] with added reactive terms [6] given by

$$||\hat{\mathbf{q}}|| = \frac{1}{2\pi}\iiint_{\Omega} \left[\rho_0|\mathbf{u}'|^2 + \frac{P_0|\rho'|^2}{\rho_0} + \frac{\rho_0^2\left(|T'|^2 + |Q'\text{Ma}^2(\gamma-1)Y_0Y'|^2\right)}{\gamma^2(\gamma-1)\text{Ma}^2 P_0}\right] r\mathrm{d}r\,\mathrm{d}x\,\mathrm{d}\theta. \tag{14}$$

By discretising the Chu norm to a weight matrix $\mathbf{W}$ we can define our norm $||\cdot||$ as the norm induced by the inner product $\langle \mathbf{x}, \mathbf{y}\rangle_{\mathbf{W}} = \mathbf{x}^H\mathbf{W}\mathbf{y}$. It will prove useful to link this norm to the standard vector 2-norm. To do this we take the Cholesky decomposition of $\mathbf{W} = \mathbf{M}^H\mathbf{M}$, letting us rephrase our optimisation in terms of the 2-norm as

$$\mathbf{f}^{\omega}_{\text{opt}} = \arg\max_{\mathbf{f}} \frac{||\mathbf{M}\mathbf{L}_{\text{out}}\mathbf{R}\mathbf{L}_{\text{in}}\mathbf{M}^{-1}\mathbf{M}\mathbf{f}||_2}{||\mathbf{M}\mathbf{f}||_2}. \tag{15}$$

The solution to this problem lies in the SVD of the matrix $\mathbf{M}\mathbf{L}_{\text{out}}\mathbf{R}\mathbf{L}_{\text{in}}\mathbf{M}^{-1}$. If we find the singular triplet corresponding to the largest singular value of this matrix it is exactly $(\sigma, \mathbf{M}\mathbf{q}^{\omega}_{\text{opt}}, \mathbf{M}\mathbf{f}^{\omega}_{\text{opt}})$, where $\sigma = ||\hat{\mathbf{q}}^{\omega}_{\text{opt}}||/||\mathbf{f}^{\omega}_{\text{opt}}||$ is the maximum growth and the optimum output is obtained from the unit-norm output given by an SVD by $\hat{\mathbf{q}}^{\omega}_{\text{opt}} = \sigma\mathbf{q}^{\omega}_{\text{opt}}$.

Since we are solving with many degrees of freedom, inverting to find the resolvent matrix is costly, hence we opt to approximate the resolvent via the long-time solution of equation (11) [6]. To make sure that our resolvent approximation is accurate enough we monitor the quantity $||\partial_t\hat{\mathbf{q}}(T)||_2/||\hat{\mathbf{q}}(T)||_2$, which should be kept small whilst keeping the total simulation time within reason. Using a final time of $T = 10$ achieves this. The adjoint equations necessary for a SVD calculation are obtained by taking the adjoint of (11) and applying a suitable final time condition. The relative error is calculated for all singular values obtained and is typically kept around 10^{-5} which equates to a percentage error of 0.001%.

To solve the singular value problem we make use of the SLEPc libraries' Lanczos SVD solver [13]. As each run of the SVD solver is costly, both in terms of time and computational resources, it is useful to extract all the information we can from a single run. It has been shown [8] that, for the SVD of a matrix $\mathbf{K}$, to first order accuracy we have the relation

$$\delta\sigma = \Re\left[\mathbf{u}^H\delta\mathbf{K}\mathbf{v}\right] \tag{16}$$

where $(\sigma, \mathbf{u}, \mathbf{v})$ is the maximal singular triplet. Using this relation with $\mathbf{K} = \mathbf{M}\mathbf{L}_{\text{out}}\mathbf{R}\mathbf{L}_{\text{in}}\mathbf{M}^{-1}$, and by assuming that the base-flow does not change significantly for a small change in parameter, we can derive gradient information

$$\frac{\partial\sigma}{\partial\omega} \approx \Im\left[\langle\mathbf{q}^{\omega}_{\text{opt}}, \mathbf{L}_{\text{out}}\mathbf{R}^2\mathbf{L}_{\text{in}}\mathbf{f}^{\omega}_{\text{opt}}\rangle_{\mathbf{W}}\right], \tag{17}$$

$$\frac{\partial\sigma}{\partial\text{Re}} \approx \Re\left[\langle\mathbf{q}^{\omega}_{\text{opt}}, \mathbf{L}_{\text{out}}\mathbf{R}\frac{\partial\mathbf{A}}{\partial\text{Re}}\mathbf{R}\mathbf{L}_{\text{in}}\mathbf{f}^{\omega}_{\text{opt}}\rangle_{\mathbf{W}}\right], \tag{18}$$

where we estimate

$$\frac{\partial\mathbf{A}}{\partial\text{Re}} \approx \frac{1}{\epsilon}\left(\mathbf{A}(\text{Re}+\epsilon) - \mathbf{A}(\text{Re})\right), \tag{19}$$

for small enough ϵ and Re kept as the value that the singular value was obtained with. Using equations (17) and (18) we can obtain parametric sensitivity information for a fraction of the cost of running another SVD. Similar equations to these have been derived in the case where the SVD problem was rephrased as an eigenvalue problem [6]. The resolvent is again approximated using (11) using the same final time T the singular value was obtained with.

5. Results

We shall define the swirl number S by [18]

$$S = \frac{\int_{r_2, x=0}^{r_1} \rho u w r^2 \, \mathrm{d}r}{r_1 \int_{r_2, x=0}^{r_1} \rho u^2 r \, \mathrm{d}r}. \tag{20}$$

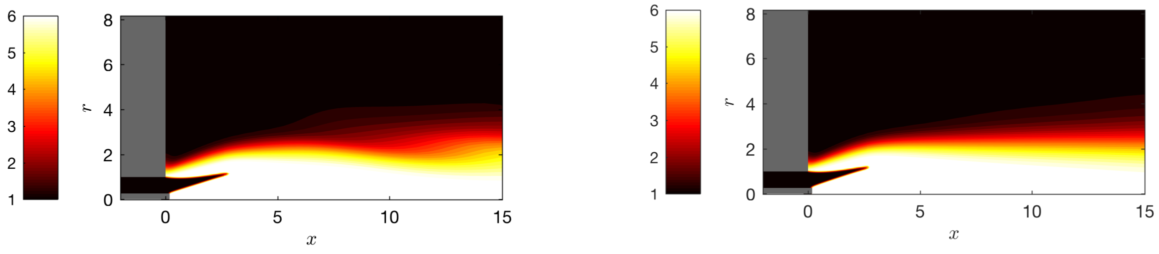

(a) $S = 0.00$ M-flame base flow (b) $S = 0.15$ M-flame base flow

Figure 2: Temperature plots of the base-flows at two different swirl numbers

Two optimisations are now carried out: one with a non-swirling base flow and another with $S = 0.15$. This low swirl number was chosen to preserve the shape of the M-flame, so that we can make an accurate comparison of the dynamics and not just observe the effect of a radically different base-flow.

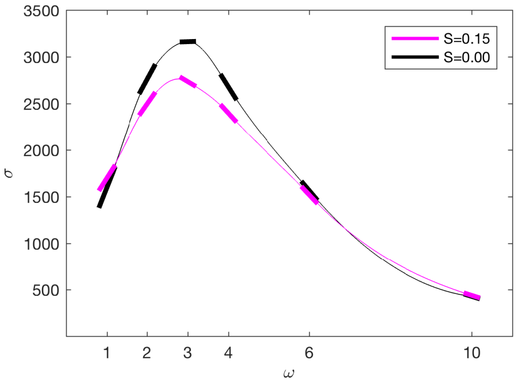

Figure 3: Optimal Growths for $S = 0.00, 0.15$. The solid lines show the gradients for the growth factors calculated. We can see that swirl decreases the growth and shifts the peak value to lower frequencies.

From figure (3) we can see that for no swirl there is a peak growth rate, obtained when $\omega = 3$. For increased swirl this maximum growth moves to lower frequencies and has a larger value, indicating that increasing the swirl inhibits the ability for the forced response to grow. Obtaining each singular value is a lengthy process taking around 5573 CPU hours to complete. By using equation (17) we can find the derivative of each singular value with respect to the forcing frequency in a third of the time of a full SVD calculation. This enables us to carry out SVDs at less points and interpolate in-between with cubic Hermite splines, providing us with a smooth and continuous picture of the data.

Now we can use equation (18) to calculate sensitivity with respect to Reynolds number. By saving the term $\mathbf{RL}_{\text{in}}\mathbf{f}^{\omega}_{\text{opt}}$ calculated during the frequency derivative routine we can reduce our simulation time to just one-sixth of a full SVD. Carrying out this procedure for no swirl and $\omega = 3$ gives a sensitivity of $\delta\sigma = 12.03\delta\text{Re}$. This calculation shows that Reynolds number is acting as an amplifier, enlarging the peak growth rate. We verify this by running an SVD for $\omega = 3$ but with the Reynolds number set higher at 1471. Using our sensitivity we can predict that the growth rate at this higher Reynolds number should be $\omega = 3162 + 10 * 12.03 = 3282$. The actual value obtained through an SVD is 3285 giving a relative error for our predicted value of 0.1%.

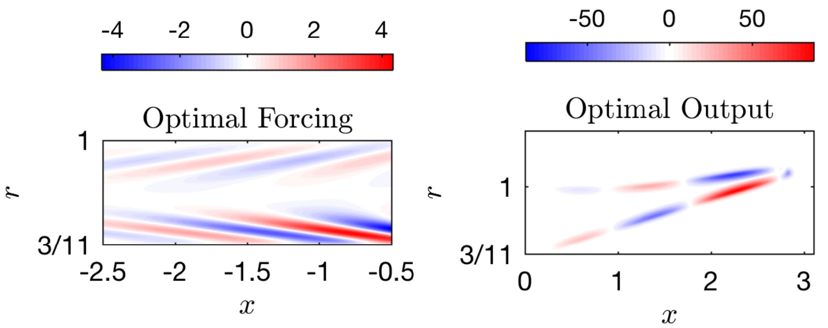

Figure 4: Real part of the optimal forcing-output shapes $\omega = 3, S = 0$. The forcing is shown as the longitudinal velocity u' whereas the output is shown as the total energy E'.

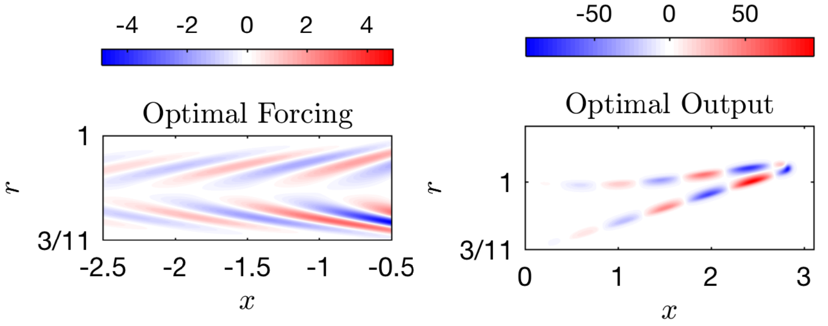

Figure 5: Real part of the optimal forcing-output (density) shapes $\omega = 6, S = 0$. The forcing is shown as the longitudinal velocity u' whereas the output is shown as the total energy E'.

Figures (4) and (5) show the form that the optimal forcing and output take for $\omega \in \{3, 6\}$. We allowed the forcing and output to consist of all flow variables; however, we can see from splitting the norm into its flow-variable components that the most efficient configuration is to force with primarily longitudinal velocity perturbations which accounts for approximately 95% of the norm. This results in an output consisting mainly of fuel mass fraction and temperature perturbations which account for around 40% each. It is not surprising that temperature and fuel mass fraction account for roughly equal amounts since the norm was designed using the fact that in simplified conditions, fuel mass fraction and temperature are equivalent [6, 10]. In both cases the forcing comes in the form of waves slanted against the mean-flow and the output is confined to the reaction layer with the waves slanted the other way. This is typical of an Orr-type mechanism for instability [19]. For a higher forcing frequency we see a shorter wavelength in both the forcing and output as well as the forcing becoming localised to the centre of the inlet. This has been seen in a previous study [6] where an optimal forcing-output was carried out for axisymmetric flow with the constraint that $w = 0$. We can also use this study to validate our growth curve for $S = 0$ since our optimal forcing has a negligible w component and we therefore get the same growth curve as if we had constrained w to zero.

6. Conclusions

A linear numerical study has been carried out to determine the maximum growth possible when a stable M-flame is submitted to harmonic flow disturbances in the inlet tube. By carrying out our analysis on two base flows with different swirl numbers we are able to see that increased swirl has a favourable effect on the flow, decreasing the peak growth and shifting it to lower frequencies. We saw that the Reynolds number enlarges the peak growth for no swirl.

Throughout our study emphasis has been put on obtaining numerical results as efficiently as possible, using a relation between a small perturbation in the growth rate to a perturbation in the resolvent to cheaply obtain sensitivity information. This enabled us to accurately and smoothly cover a large range of frequencies with limited singular value calculations. We were also able to obtain the effect that the Reynolds number has on the peak growth rates for a sixth of the cost of a full simulation.

REFERENCES

1. Yang, V. and Liewen, T., *Combustion Instabilities In Gas Turbine Engines: Operational Experience, Fundamental Mechanisms, and Modeling*, American Institute of Aeronautics and Astronautics (2005).
2. Culick, F. E. C., (1996), *Combustion Instabilities in Propulsion Systems*. Springer Netherlands.
3. Rayleigh, L. The explanation of certain acoustical phenomena, *Nature*, **18**, 319–321, (1878).
4. Huang, Y. and Yang, V. Dynamics and stability of lean-premixed swirl-stabilized combustion, *Progress in Energy and Combustion Science*, **35** (4), 293–364, (2009).
5. Huang, Y. and Yang, V. Effect of swirl on combustion dynamics in a lean-premixed swirl-stabilized combustor, *Proceedings of the Combustion Institute*, **30**, 1775–1782, (2005).
6. Blanchard, M., *Linear and nonlinear dynamics of laminar premixed flames submitted to flow oscillations*, Ph.D. thesis, Ecole polytechnique, (2015).
7. Fosas De Pando, M., Sipp, D. and Schmid, P. J. Efficient evaluation of the direct and adjoint linearized dynamics from compressible flow solvers, *Journal of Computational Physics*, **231** (23), 7739–7755, (2012).
8. Fosas de Pando, M., Schmid, P. and Lele, S. Parametric sensitivity for large-scale aeroacoustic flows, *Center for Turubulence Research, Proceedings of the Summer program*, (2014).
9. Blanchard, M., Schmid, P. J., Sipp, D. and Schuller, T. Pressure wave generation from perturbed premixed flames, *Journal of Fluid Mechanics*, **797**, 231–246, (2016).
10. Poinsot, T. and Veynante, D., *Theoretical and numerical combustion*, Aquaprint, 3 edn. (2012).
11. Williams, F., *Combustion theory*, Addison-Wesley, 2 edn. (1988).
12. Balay, S., et al., (2016), *PETSc Web page*. `http://www.mcs.anl.gov/petsc`.
13. Hernandez, V., Roman, J. E. and Vidal, V. SLEPc: A scalable and flexible toolkit for the solution of eigenvalue problems, *ACM Trans. Math. Software*, **31** (3), 351–362, (2005).
14. Lodato, G., Domingo, P. and Vervisch, L. Three-dimensional boundary conditions for direct and large-eddy simulation of compressible viscous flows, *Journal of Computational Physics*, **227** (10), 5105 – 5143, (2008).
15. Berland, J., Bogey, C., Marsden, O. and Bailly, C. High-order, low dispersive and low dissipative explicit schemes for multiple-scale and boundary problems, *Journal of Computational Physics*, **224** (2), 637 – 662, (2007).
16. Åkervik, E., Brandt, L., Henningson, D. S., Hœpffner, J., Marxen, O., Schlatter, P., Åkervik, E., Brandt, L., Henningson, D. S. and Hœpffner, J. Steady solutions of the Navier-Stokes equations by selective frequency damping Steady solutions of the Navier-Stokes equations by selective frequency damping, *Physics of Fluids*, **18**, (2006).
17. Chu, B.-T. On the energy transfer to small disturbances in fluid flow (part i), *Acta Mechanica*, **1** (3), 215–234, (1965).
18. Gupta, A. K., Lilley, D. G. and Syred, N., *Swirl flows*, Abacus Press (1984).
19. Orr, W. M. The Stability or Instability of the Steady Motions of a Perfect Liquid and of a Viscous Liquid. Part II: A Viscous Liquiditle, *Proceedings of the Royal Irish Academy. Section A: Mathematical and Physical Sciences*, **27**, 69–138, (1907).